JOURNAL OF MAGNETIC RESONANCE **100,** 282–302 (1992)

Gradient-Enhanced Heteronuclear Correlation Spectroscopy. Theory and Experimental Aspects

JESÚS RUIZ-CABELLO,* GEERTEN W. VUISTER,† CHRIT T. W. MOONEN,‡ PETER VAN GELDEREN,‡,§ JACK S. COHEN,* AND PETER C. M. VAN ZIJL*,‖

*Georgetown University Medical School, Department of Pharmacology, 4 Research Court, Rockville, Maryland 20850; †Laboratory of Chemical Physics, NIDDK, National Institutes of Health, Building 2, Bethesda, Maryland 20892; ‡In Vivo NMR Research Center, BEIP, NCRR, National Institutes of Health, Building 10, Rm. B1D-125, Bethesda, Maryland 20892; and §Department of Physics, Technical University Delft, Delft, The Netherlands

Received December 26, 1991; revised March 2, 1992

A detailed theoretical and experimental treatment is given for gradient-enhanced heteronuclear correlation spectroscopy. Both multiple-quantum and single-quantum sequences are described. In addition to a comparison with conventional experiments using phase cycling, the effects of different gradient combinations are examined with respect to artifacts occurring in the heteronuclear dimension. The influence of gradient performance and diffusion on sensitivity is discussed. Approaches to attain phase-sensitive spectra are also analyzed. © 1992 Academic Press, Inc.

Coherence selection using gradients provides an alternative over phase cycling (*1*). Recent technological progress in the design of high-quality shielded gradients has stimulated publication of a number of homonuclear (*2–9*) and heteronuclear (*10–13*) gradient-enhanced experiments. Of special importance for high-resolution NMR are multidimensional gradient-enhanced proton-detected heteronuclear experiments (*12, 13*). They provide single-scan (i.e., one scan per t_1 increment) acquisition with frequency-independent water suppression (*14*) and allow detection of exchangeable protons (*13*). These methods have been shown to facilitate 2D acquisition in minutes (*12a, 13a*) and reduction of 3D experiment time from days to hours (*12b, 13b*). However, despite the inherent simplicity of these techniques, their practical application is not yet straightforward and strongly depends on factors like hardware performance and chosen gradient combinations. The purpose of this paper is to discuss these factors and compare these new techniques with conventional methods using phase cycling. We restrict ourselves to the heteronuclear multiple-quantum-coherence [HMQC (*15*)] and single-quantum-coherence [HSQC (*16*)] experiments. All principles are demonstrated for the simple compound [$^{13}C_1$]glucose. The principles outlined also apply to variations of the conventional HMQC and HSQC schemes (*17, 18*).

‖ To whom correspondence should be addressed at present address: Johns Hopkins University Medical School, Department of Radiology, MRI 110, 600 N. Wolfe Street, Baltimore, Maryland 21287.

0022-2364/92 $5.00

DOI of original item: doi: 10.1016/0022-2364(92)90262-6

THEORY

We describe the coherence-selection process with gradients using the coherence-transfer formalism (*19, 20*), in which transverse magnetization is described by the two spin-rotation components I^+ and I^-. In this formalism, the evolution of magnetization in the presence of magnetic field gradients can be conveniently described in terms of an acquired phase (*5c, 8, 9, 12–14, 21*). The definitions used in this formalism differ slightly in different publications and to avoid confusion we have given all our definitions and evolution rules in the Appendix. Also, proton chemical shifts are refocused in HSQC and HMQC experiments and are therefore not included in the evolution description of the preparation and refocusing periods. Since quadrature detection is used, only one of the spin-rotation components is detected. We conventionally choose this to be I^-.

When using gradients, the phase ϕ acquired due to evolution of a spin I of coherence order p depends on the spatial position $\mathbf{r}$ of the spin in the sample:

$$I^p \rightarrow I^p e^{-ip\phi(\mathbf{r})} = I^p e^{-ip\gamma_I(\mathbf{G}\cdot\mathbf{r})\tau}. \qquad [1]$$

$\mathbf{G}$ denotes the gradient vector, τ is the duration of gradient application, and γ_I is the nuclear gyromagnetic ratio for spin I. Since the signal S is measured over the complete sample, application of enough gradient strength causes a random distribution of phases and the signal is dispersed:

$$S \sim \int e^{-ip\gamma_I(\mathbf{G}\cdot\mathbf{r})\tau} dr \rightarrow 0 \qquad \text{for } G \rightarrow \infty. \qquad [2]$$

Thus, signal for a certain coherence pathway is refocused only when the sum of the effects of all applied coherence-selection gradients G_i in directions α ($\alpha = x, y, z$) is zero for this pathway:

$$\sum_i p\gamma_I(\mathbf{G}\cdot\mathbf{r})_i\tau_i = \sum_i p\gamma_I\Big(\sum_\alpha G_\alpha r_\alpha\Big)_i\tau_i = 0. \qquad [3]$$

In the description of the HMQC and HSQC sequences, we use three selection gradients (G_1–G_3). For simplicity we denote the magnitude of the vector sum over all three gradient directions by Gr and apply only gradients of equal length $\tau_i = \tau$. We assume complete signal dispersion when a gradient term is left uncompensated in the final formula for the signal intensity. In practice this can of course be accomplished only when sufficient gradient strength is available. Equations [1]–[3] also show that dephasing by gradients depends on the nuclear gyromagnetic ratios. Thus, in heteronuclear experiments, the ratio of the γ values of the different nuclei involved becomes important.

In the next paragraphs we analyze the gradient-enhanced versions of the HMQC (ge-HMQC) and HSQC (ge-HSQC) sequences. The calculation is for an AX system and relaxation is ignored as usual. In the treatment we describe proton magnetization by I and heteronuclear magnetization by S. The origin of frequencies and gyromagnetic ratios is indicated by subscripts H and X for a proton and the X nucleus, respectively. The heteronuclear scalar coupling constant is denoted J.

HMQC

Figure 1 shows the pulse sequence and coherence pathways for the gradient-enhanced HMQC experiment. The pathways were calculated following the rules in the Appendix.

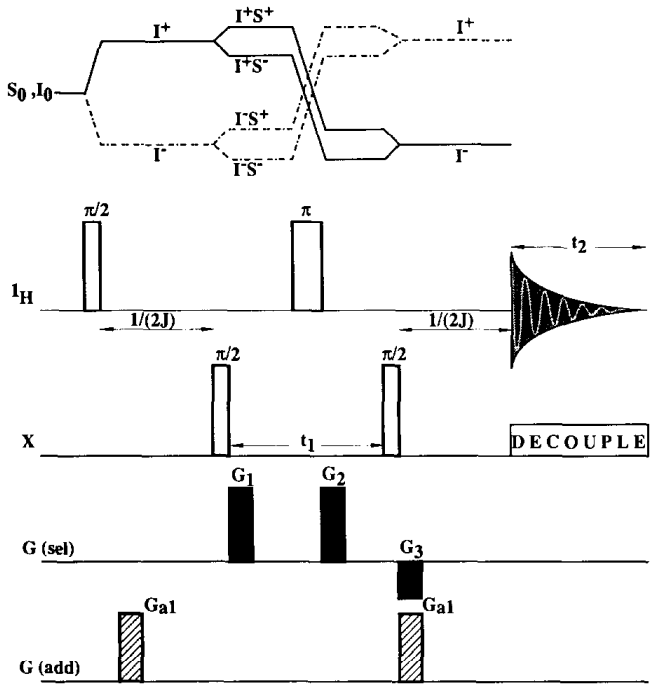

FIG. 1. Coherence pathways and pulse sequence (bottom) for gradient-enhanced HMQC spectroscopy (ge-HMQC). The phase of all RF pulses is indifferent. G(sel) denotes gradients for coherence selection. G(add) denotes additional gradients for eliminating water signal resulting from imperfections in the proton π pulse.

The sequence consists of a $\pi/2$ proton excitation pulse followed by two $\pi/2$ carbon pulses for transfer of magnetization to the heteronucleus and back to ^{1}H. The π proton pulse in the middle of the sequence refocuses the ^{1}H chemical shift at the start of the acquisition. After the preparation time of length $1/(2J)$, zero-quantum (I^+S^-, I^-S^+) and double-quantum (I^+S^+, I^-S^-) coherences are generated. The effect of the proton π pulse is to switch I^+ for I^-, interchanging double-quantum coherence (DQC) and zero-quantum coherence (ZQC). This transfer is represented by the crossing lines in Fig. 1. As a result the proton chemical shift is refocused during t_1 and the evolution for the heteronucleus is pseudo-single quantum (*15b, 15c*). For instance, for the t_1 pathway $I^+S^+ \rightarrow I^-S^+$, the effective chemical-shift evolution is

$$e^{-i(\omega_H+\omega_X)t_1/2}e^{-i(-\omega_H+\omega_X)t_1/2} = e^{-i\omega_X t_1}. \quad [4]$$

When one selects only pathways that result in single-quantum proton magnetization I^- after the second carbon pulse, the following phases are acquired during t_1 for the DQ $\rightarrow$ ZQ and ZQ $\rightarrow$ DQ pathways, respectively:

$$e^{-i\phi}(I^+S^+ \rightarrow I^-S^+) = e^{-i(\omega_X)t_1}e^{-i(\gamma_H+\gamma_X)G_1r\tau}e^{-i(-\gamma_H+\gamma_X)G_2r\tau} \quad [5a]$$

$$e^{-i\phi}(I^+S^- \rightarrow I^-S^-) = -e^{-i(-\omega_X)t_1}e^{-i(\gamma_H-\gamma_X)G_1r\tau}e^{-i(-\gamma_H-\gamma_X)G_2r\tau}. \quad [5b]$$

The phase acquired during the gradient pulse G_3 in the refocusing period before acquisition (I^- evolution) is $-\gamma_H G_3 r\tau$. Thus, for gradients of equal duration, signal rephasing and detection are achieved if

$$(\gamma_H + \gamma_X)G_1 + (-\gamma_H + \gamma_X)G_2 - \gamma_H G_3 = 0 \quad [6a]$$

$$(\gamma_H - \gamma_X)G_1 + (-\gamma_H - \gamma_X)G_2 - \gamma_H G_3 = 0. \quad [6b]$$

As a consequence, five different dephasing–rephasing conditions can be distinguished for the gradient-enhanced HMQC (Table 1):

Pseudo-SQ ^{13}C dephasing/SQ ^1H rephasing. This occurs for $G_1 = G_2$, where, due to the canceling proton contributions, dephasing is proportional to γ_X. The solution for this condition is accomplished if

$$G_1 = G_2 = \pm \frac{\gamma_H}{2\gamma_X} G_3. \quad [7]$$

Thus, for a ^{13}C–^1H system ($\gamma_H/\gamma_X = 4$), the gradient ratio $G_1{:}G_2{:}G_3 = 2{:}2{:}+1$ rephases the $I^+S^+ \rightarrow I^-S^+ \rightarrow I^-$ pathway, while the 2:2:−1 combination rephases $I^+S^- \rightarrow I^-S^- \rightarrow I^-$. These pathways correspond to positive (ω_X) and negative ($-\omega_X$) heteronuclear evolution during t_1, respectively.

ZQ dephasing/SQ ^1H rephasing. This occurs for the following gradient combinations, where dephasing during one-half of t_1 is proportional to $\gamma_H - \gamma_X$:

$$G_1 = 0, \qquad G_2 = -\frac{\gamma_H}{\gamma_H - \gamma_X} G_3 \quad [8a]$$

$$G_2 = 0, \qquad G_1 = +\frac{\gamma_H}{\gamma_H - \gamma_X} G_3. \quad [8b]$$

Hence, for ^{13}C–^1H, the ratio 0:4:−3 rephases the $I^+S^+ \rightarrow I^-S^+ \rightarrow I^-$ pathway, while 4:0:3 rephases $I^+S^- \rightarrow I^-S^- \rightarrow I^-$.

DQ dephasing/SQ ^1H rephasing. The condition for rephasing is

$$G_1 = 0, \qquad G_2 = -\frac{\gamma_H}{\gamma_H + \gamma_X} G_3 \quad [9a]$$

$$G_2 = 0, \qquad G_1 = +\frac{\gamma_H}{\gamma_H + \gamma_X} G_3. \quad [9b]$$

Thus, in the ^{13}C–^1H case, a 4:0:5 gradient ratio selects $I^+S^+ \rightarrow I^-S^+ \rightarrow I^-$, while 0:4:−5 rephases $I^+S^- \rightarrow I^-S^- \rightarrow I^-$.

TABLE 1

Gradient Ratios for Selecting Certain Coherence Pathways during t_1 in Gradient-Enhanced HMQC and HSQC Spectroscopy

	Pathway	f_1	$G_1/G_3 = G_2/G_3$	G_1	G_2/G_3	G_1/G_3	G_2	G_1/G_2	G_3
HMQC	$I^+S^+ \rightarrow I^-S^+$	ω_X	$(\gamma_H/2\gamma_X)$	0	$-\gamma_H/(\gamma_H - \gamma_X)$	$\gamma_H/(\gamma_H + \gamma_X)$	0	$(\gamma_H - \gamma_X)/(\gamma_H + \gamma_X)$	0
	$I^+S^- \rightarrow I^-S^-$	$-\omega_X$	$-(\gamma_H/2\gamma_X)$	0	$-\gamma_H/(\gamma_H + \gamma_X)$	$\gamma_H/(\gamma_H - \gamma_X)$	0	$(\gamma_H + \gamma_X)/(\gamma_H - \gamma_X)$	0
HSQC	$S^+ \rightarrow S^+$	ω_X	$-(\gamma_H/2\gamma_X)$	0	$-(\gamma_H/\gamma_X)$	$-(\gamma_H/\gamma_X)$	0	NA	NA
	$S^- \rightarrow S^-$	$-\omega_X$	$(\gamma_H/2\gamma_X)$	0	(γ_H/γ_X)	(γ_H/γ_X)	0	NA	NA

DQ dephasing/ZQ rephasing. The condition for rephasing is

$$G_3 = 0, \qquad G_1 = \frac{\gamma_H - \gamma_X}{\gamma_H + \gamma_X} G_2. \qquad [10]$$

Thus, in the $^{13}C-^{1}H$ case, a 3:5:0 gradient ratio selects $I^+S^+ \rightarrow I^-S^+ \rightarrow I^-$.

ZQ dephasing/DQ rephasing. The condition for rephasing is

$$G_3 = 0, \qquad G_1 = \frac{\gamma_H + \gamma_X}{\gamma_H - \gamma_X} G_2. \qquad [11]$$

In the $^{13}C-^{1}H$ case, a 5:3:0 gradient ratio selects $I^+S^- \rightarrow I^-S^- \rightarrow I^-$.

The additional gradients G_{a1} in Fig. 1 are not of importance for coherence selection, but assist in removal of water signal that may be excited by an imperfect π pulse during t_1.

HSQC

Figure 2 shows the pulse sequence and coherence-transfer pathways for gradient-enhanced heteronuclear single-quantum spectroscopy. This experiment employs an INEPT (*22*) for transfer to the heteronucleus and a reverse INEPT to return to observable proton magnetization. The three π pulses refocus the ^{1}H chemical shift, and

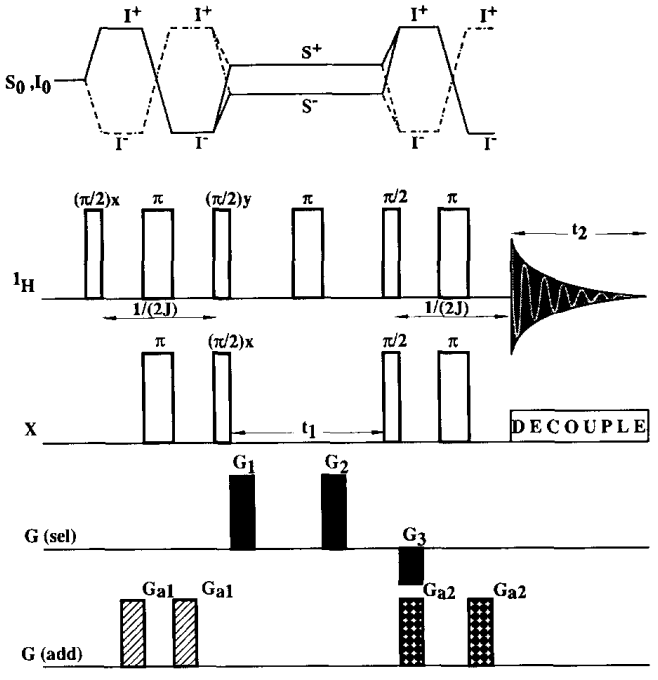

FIG. 2. Coherence pathways and pulse sequence (bottom) for gradient-enhanced HSQC spectroscopy (ge-HSQC). The phase of the proton transfer pulse after $1/(2J)$ is perpendicular to the first pulse; the phase of the carbon-transfer pulse is equal to that of the first pulse. Chemical-shift refocusing is necessary after preparation and, contrary to the HMQC sequence, no gradients can be placed around t_1. The phases of the other RF pulses are indifferent. G(sel) and G(add) are defined as in the legend to Fig. 1.

the π pulse during t_1 also refocuses the heteronuclear couplings in this period. After the preparation time only single-quantum magnetization (S^+, S^-) is generated.

Unlike in the HMQC sequence, there is no change of coherence order during t_1 (see Figs. 1 and 2). Considering gradients on both sides of the central π_H pulse, the acquired phases for the two selected pathways are

$$e^{-i\phi}(S^+ \rightarrow S^+) = e^{-i(\omega_X)t_1}e^{-i(\gamma_X)G_1r\tau}e^{-i(\gamma_X)G_2r\tau} \quad [12a]$$

$$e^{-i\phi}(S^- \rightarrow S^-) = -e^{-i(-\omega_X)t_1}e^{-i(-\gamma_X)G_1r\tau}e^{-i(-\gamma_X)G_2r\tau}. \quad [12b]$$

Since the π_H pulse has no effect on the ^{13}C chemical-shift evolution, all three gradient combinations have the same effect as a single gradient pulse somewhere during t_1. In the HSQC (Fig. 2), gradient rephasing occurs before the π pulses during the refocusing period. Because I^+ is evolving there, a phase of $\gamma_H G_3 r\tau$ is acquired. Thus, rephasing is assured when

$$\gamma_X(G_1 + G_2) + \gamma_H G_3 = 0 \quad [13a]$$

$$-\gamma_X(G_1 + G_2) + \gamma_H G_3 = 0. \quad [13b]$$

This corresponds to

$$G_1 + G_2 = \mp \frac{\gamma_H}{\gamma_X} G_3. \quad [14]$$

Therefore, for a ^{13}C–^1H system, the 2:2:−1, 0:4:−1, and 4:0:−1 gradient ratios rephase the $S^+ \rightarrow S^+ \rightarrow I^+ \rightarrow I^-$ coherence pathway, while the 2:2:1, 0:4:1, and 4:0:1 ratios select $S^- \rightarrow S^- \rightarrow I^+ \rightarrow I^-$ (cf. Table 1). The only valid solution for $G_3 = 0$ is when the two other gradients are also zero, which is not useful for dephasing of unwanted coherences.

The additional gradients ($G_{a1,2}$) around the π pulses in the preparation and refocusing periods are useful for removing solvent signals excited by imperfect π pulses. However, they cannot remove all of the additional coherence pathways for coupled spins caused by the $\pi/2$ character of these pulses.

EXPERIMENTAL

Recent studies have demonstrated the feasibility of using gradient-enhanced HMQC (*13, 14*) and HSQC (*13*) for macromolecules at low concentration in H_2O solution. For this paper, discussing the principles of the method, we apply the sequences to the simple case of 100 m*M* $^{13}C_1$-enriched glucose (Cambridge Isotopes) in 99% D_2O.

All experiments were performed on a GE PSG wide-bore 400 MHz NMR spectrometer, equipped with shielded gradients coils. The length of the gradient pulses was 1.7 ms. The postgradient delay was 50 μs, leading to a minimum t_1 of 3.5 ms. Unless mentioned otherwise, the gradient strengths used per unit were 0.026 T/m (x and z axes). The experiments without gradients used the phase-cycling schemes in Table 2 (*23*).

All experiments were recorded with four dummy scans, a spectral width of 5000 Hz, and a predelay of 1 s. All 1D spectra were eight-scan FIDs of 2048 complex points, processed with a 2 Hz exponential line broadening. Single-scan 2D experiments with

TABLE 2

Phase-Cycle Schemes Used for HMQC and HSQC Spectroscopy (*23*)

Nucleus					
		HMQC			
$(\pi/2)$	H	0	0		
$(\pi/2)$	X	0	180°		
(π)	H	180°	180°		
$(\pi/2)$	X	0	0		
Receiver		0	180°		
		HSQC			
$(\pi/2)$	H	0	0	0	0
(π)	H, X	0	0	0	0
$(\pi/2)$	H	90°	90°	90°	90°
$(\pi/2)$	X	0	180°	0	180°
(π)	H	180°	180°	180°	180°
$(\pi/2)$	H	270°	270°	270°	270°
$(\pi/2)$	X	0	0	180°	180°
(π)	H, X	0	0	0	0
Receiver		0	180°	180°	0

gradients consisted of 128 (t_1) FIDs of 256 complex points. For comparison with conventional phase-cycled experiments the number of scans was adjusted to the number of phase-cycle steps. Both magnitude- and phase-sensitive spectra were recorded. Phase-sensitive gradient experiments were obtained by cycling G_3 for alternating scans. For HMQC experiments with $G_1 = G_2$, the sign of G_3 was cycled, while for experiments with $G_1 = 0$ or $G_2 = 0$, G_3 was cycled between -3 and -5, and 3 and 5, respectively. For the phase-sensitive HSQC, the sign of G_3 was cycled for alternating scans. Quadrature detection in the f_1 dimension was obtained by the States method (*24*). The DC offset in all experiments was removed by fitting the final 50 points of both real and imaginary parts of the FID and averaging them to obtain the zero level. All 2D data were processed with sine-bell windows shifted by 90° before Fourier transformation in t_1 and t_2. The data were zero-filled once in t_1 prior to Fourier transformation.

RESULTS AND DISCUSSION

Sensitivity Comparison between Gradient Methods and Conventional Experiments

Table 3 compares the proton signal intensities for ge-HMQC, ge-HSQC, and the conventional phase-cycled experiments. These intensities reflect the integrated FID, which is the sum of absolute values of all points in the real and imaginary FID. For each sequence, a loss of a factor of 2 with respect to phase cycling is found. This is expected, since both pathways are detected in the conventional experiments and only one in the gradient experiments. Thus, when a two-scan phase-sensitive method is

TABLE 3

Comparison of Signal Intensities between Conventional (Phase-Cycle) Coherence-Selection Experiments and Methods Based on Gradient Selection

Pulse sequence	Phase cycle	$G_1 = G_2$		$G_1 = 0$		$G_2 = 0$		$G_3 = 0$	
		a	*b*	*a*	*b*	*a*	*b*	*a*	*b*
HMQC	1112 ± 15	588 ± 10	607 ± 13	578 ± 24	579 ± 8	553 ± 14	520 ± 22	470 ± 6	563 ± 9
HSQC	806 ± 5	460 ± 11	399 ± 6	418 ± 6	367 ± 10	461 ± 7	467 ± 9		

Note. Values are integrated FIDs (see text); eight scans and four dummy scans were taken for all experiments. Additional gradients (see Figs. 1 and 2) were turned off. Numbers are the average of five measurements; the error is the standard deviation from mean. Situation *a* is for the $S^+ \rightarrow I^-$ pathway; *b* is for $S^- \rightarrow I^-$.

used for indirect detection in a phase-cycling experiment, signal intensities are equal to a two-scan gradient magnitude experiment, since one component is removed.

For both phase-cycled and gradient-enhanced experiments, signal intensities are higher for multiple-quantum experiments, mainly because of the smaller number of RF pulses. This makes the HSQC sequence more sensitive to B_1 inhomogeneity. Most signal loss is due to imperfections in the π pulses during preparation and J refocusing, where either the gradient pair or phase cycling removes improperly refocused signals. When magnitude spectra are obtained, the π pulses during the last refocusing period can in principle be deleted.

It should be noted here that, despite a loss in resolution, the gradient experiment has advantages in many situations. For instance, in conventional experiments using RF presaturation for water suppression, signal of exchangeable protons may be lost. In the gradient-enhanced experiments, the time for possible magnetization transfer from saturated (dephased) water to exchangeable protons is very short, allowing their efficient detection (*13a*). When signal-to-noise is high enough, gradient experiments are advantageous for studying kinetics. Also, experimental setup time for water suppression is negligible and water suppression is frequency independent (*10–14*).

Artifacts in the Heteronuclear Dimension

The presence of artifacts in the t_1 dimension was studied in both gradient and conventional phase-cycling experiments. In both cases, most artifactual cross peaks arise due to excitation of the additional coherence pathways when the central proton π pulse is inaccurate. However, depending on the gradient dephasing–rephasing pathway chosen, these artifacts may or may not become visible. Of course their presence, even if not detected, results in signal loss. As a demonstration, Figs. 3a–3c show 2D HMQC spectra of glucose, recorded with a central $\pi/2$ proton pulse and gradient selections 2:2:−1, 0:4:−3, and 4:0:3, respectively. Clearly the results are quite different. This can be explained when calculating the signal intensities using a flip angle β instead of π for the central proton pulse:

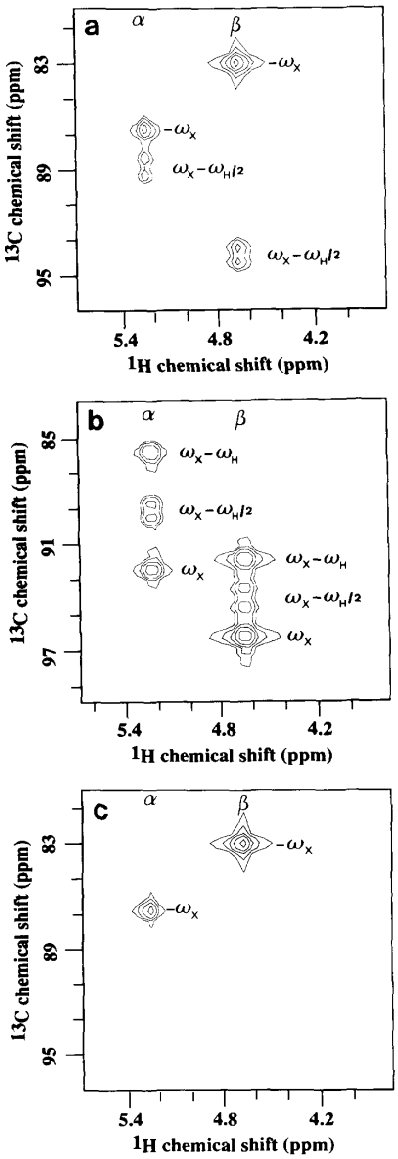

FIG. 3. Magnitude 2D ge-HMQC spectra of [$^{13}C_1$]glucose (100 mM) in 99% D_2O, showing the effect of a proton pulse with $\pi/2$ character in the middle of t_1. The gradient ratios G_1:G_2:G_3 are: (a) 2:2:−1, (b) 0:4:−3, and (c) 4:0:3. The ^{13}C offset is 90 ppm; the ^{1}H offset 3.5 ppm.

$$e^{-i\phi}(I^+S^+ \rightarrow I^-S^+) = -1/2(\cos\beta - 1)e^{-i(\omega_X)t_1}e^{-i(\gamma_H+\gamma_X)G_1r\tau}e^{-i(-\gamma_H+\gamma_X)G_2r\tau} \quad [15a]$$

$$e^{-i\phi}(I^+S^- \rightarrow I^-S^-) = +1/2(\cos\beta - 1)e^{-i(-\omega_X)t_1}e^{-i(\gamma_H-\gamma_X)G_1r\tau}e^{-i(-\gamma_H-\gamma_X)G_2r\tau} \quad [15b]$$

$$e^{-i\phi}(I^-S^+ \rightarrow I^-S^+) = +1/2(\cos\beta + 1)e^{-i(-\omega_H+\omega_X)t_1}e^{-i(-\gamma_H+\gamma_X)G_1r\tau}e^{-i(-\gamma_H+\gamma_X)G_2r\tau} \quad [15c]$$

$$e^{-i\phi}(I^-S^- \rightarrow I^-S^-) = -1/2(\cos\beta + 1)e^{-i(-\omega_H-\omega_X)t_1}e^{-i(-\gamma_H-\gamma_X)G_1r\tau}e^{-i(-\gamma_H-\gamma_X)G_2r\tau}. \quad [15d]$$

This expression equals Eq. [5] for $\beta = \pi$. The artifacts in Eqs. [15c] and [15d] correspond to pathways in which the sign of the proton coherence is not changed by the central pulse. It can be seen at once that the dephasing condition for these artifacts is the same during G_1 and G_2. Thus, these artifacts are visible if

$$(-\gamma_H + \gamma_X)(G_1 + G_2) - \gamma_H G_3 = 0 \quad [16a]$$

$$(-\gamma_H - \gamma_X)(G_1 + G_2) - \gamma_H G_3 = 0. \quad [16b]$$

These equations and Eq. [6] only have identical solutions for $G_1{:}G_2{:}G_3 = 0{:}4{:}-3$ and $0{:}4{:}-5$, since these combinations are independent of the effect of the central proton pulse. In addition to these expected artifacts, extra cross peaks at $\omega_X - \omega_H/2$ and $-\omega_X$

TABLE 4

Normal Frequencies and Possible Artifacts in f_1 for Gradient-Enhanced HMQC and HSQC Spectroscopy

	HMQC		HSQC	
	$G_3 = 1$	$G_3 = -1$	$G_3 = -1$	$G_3 = 1$
$G_1 = G_2 = 2$	ω_X	$-\omega_X$ $\omega_X - \omega_H/2$	ω_X[a] $-\omega_X + \omega_H/2$	$-\omega_X$[a] $\omega_X - \omega_H/2$
	$G_3 = -3$	$G_3 = -5$		
$G_1 = 0, G_2 = 4$	ω_X $\omega_X - \omega_H/2$ $\omega_X - \omega_H$	$-\omega_X$ $-\omega_X - \omega_H/2$ $-\omega_X - \omega_H$	ω_X[a]	$-\omega_X$[a]
	$G_3 = 5$	$G_3 = 3$		
$G_1 = 4, G_2 = 0$	ω_X	$-\omega_X$	ω_X[a] $\omega_X + \omega_H/2$ $\omega_X - \omega_H/2$	$-\omega_X$[a] $-\omega_X + \omega_H/2$ $-\omega_X - \omega_H/2$
	$G_1 = 3, G_2 = 5$	$G_1 = 5, G_2 = 3$		
$G_3 = 0$	ω_X	$-\omega_X$		

[a] These peaks are singlets for a normal π pulse and doublets when this pulse has $\pi/2$ character.

$-\omega_H/2$ were found for some of the gradient combinations (Table 4, Fig. 3). Their origin can be traced back from these frequencies. Since only I^- is detected, the proton magnetization after the last proton pulse in the middle of t_1 must be I^-. The carbon magnetization does not change due to this proton pulse and is the same during t_1. Since the frequency of the cross peak has an offset of $\omega_H/2$, there is only proton evolution during one-half of t_1. Thus the pathways causing these artifactual cross peaks must be $S^+ \rightarrow I^-S^+ \rightarrow I^-$ and $S^- \rightarrow I^-S^- \rightarrow I^-$. This conclusion should agree with the occurrence of artifacts for only some of the gradient combinations. The rephasing conditions for the two pathways are

$$\gamma_X G_1 + (-\gamma_H + \gamma_X)G_2 - \gamma_H G_3 = 0 \quad [17a]$$

$$-\gamma_X G_1 + (-\gamma_H - \gamma_X)G_2 - \gamma_H G_3 = 0. \quad [17b]$$

Equation [17a] is solved for $G_1:G_2:G_3 = 2:2:-1$ and $0:4:-3$ and artifacts are indeed found at $\omega_X - \omega_H/2$ for these gradient combinations (Table 4, Figs. 3a and 3b). Equation [17b] is satisfied for $G_1:G_2:G_3 = 0:4:-5$, in agreement with the cross peak found at $-\omega_X - \omega_H/2$ for this gradient ratio. The occurrence of these artifacts due to a coherence pathway for magnetization only first excited by the first carbon pulse is a consequence of bad B_1 homogeneity.

In the HSQC experiment, four additional pathways can be attained if the central proton pulse in t_1 has 90° character. This is more than that in the HMQC, since a central $\pi/2$ pulse excites I^+ and I^- magnetization, which are both transferred to I^- by the $\pi/2$ proton pulse after t_1. The corresponding signal intensities for the six pathways are

$$e^{-i\phi}(S^+ \rightarrow S^+) = -\cos\beta e^{-i(\omega_X)t_1}e^{-i(\gamma_X)G_1r\tau}e^{-i(\gamma_X)G_2r\tau} \quad [18a]$$

$$e^{-i\phi}(S^+ \rightarrow I^+S^+) = -1/2\sin\beta e^{-i(\omega_H/2+\omega_X)t_1}e^{-i(\gamma_X)G_1r\tau}e^{-i(\gamma_H+\gamma_X)G_2r\tau} \quad [18b]$$

$$e^{-i\phi}(S^+ \rightarrow I^-S^+) = +1/2\sin\beta e^{-i(-\omega_H/2+\omega_X)t_1}e^{-i(\gamma_X)G_1r\tau}e^{-i(-\gamma_H+\gamma_X)G_2r\tau} \quad [18c]$$

$$e^{-i\phi}(S^- \rightarrow S^-) = +\cos\beta e^{-i(-\omega_X)t_1}e^{-i(-\gamma_X)G_1r\tau}e^{-i(-\gamma_X)G_2r\tau} \quad [18d]$$

$$e^{-i\phi}(S^- \rightarrow I^+S^-) = +1/2\sin\beta e^{-i(\omega_H/2-\omega_X)t_1}e^{-i(-\gamma_X)G_1r\tau}e^{-i(\gamma_H-\gamma_X)G_2r\tau} \quad [18e]$$

$$e^{-i\phi}(S^- \rightarrow I^-S^-) = -1/2\sin\beta e^{-i(-\omega_H/2-\omega_X)t_1}e^{-i(-\gamma_X)G_1r\tau}e^{-i(-\gamma_H-\gamma_X)G_2r\tau}. \quad [18f]$$

This equation equals Eq. [12] for $\beta = \pi$. Artifacts are refocused when

$$\gamma_X G_1 + (\gamma_H + \gamma_X)G_2 + \gamma_H G_3 = 0 \quad [19a]$$

$$\gamma_X G_1 + (-\gamma_H + \gamma_X)G_2 + \gamma_H G_3 = 0 \quad [19b]$$

$$-\gamma_X G_1 + (\gamma_H - \gamma_X)G_2 + \gamma_H G_3 = 0 \quad [19c]$$

$$-\gamma_X G_1 + (-\gamma_H - \gamma_X)G_2 + \gamma_H G_3 = 0. \quad [19d]$$

It is clear that artifacts and correct cross peaks are refocused simultaneously for $G_2 = 0$, which is found experimentally (Table 4, Fig. 4c). Equations [19b] and [19c] have additional solutions for $G_1:G_2:G_3 = 2:2:1$ and $2:2:-1$, respectively. Indeed artifacts for these gradient combinations are found at the expected frequencies. It is interesting to see that, when $\beta = \pi/2$, the cross peaks (for both isomers) at the correct frequencies

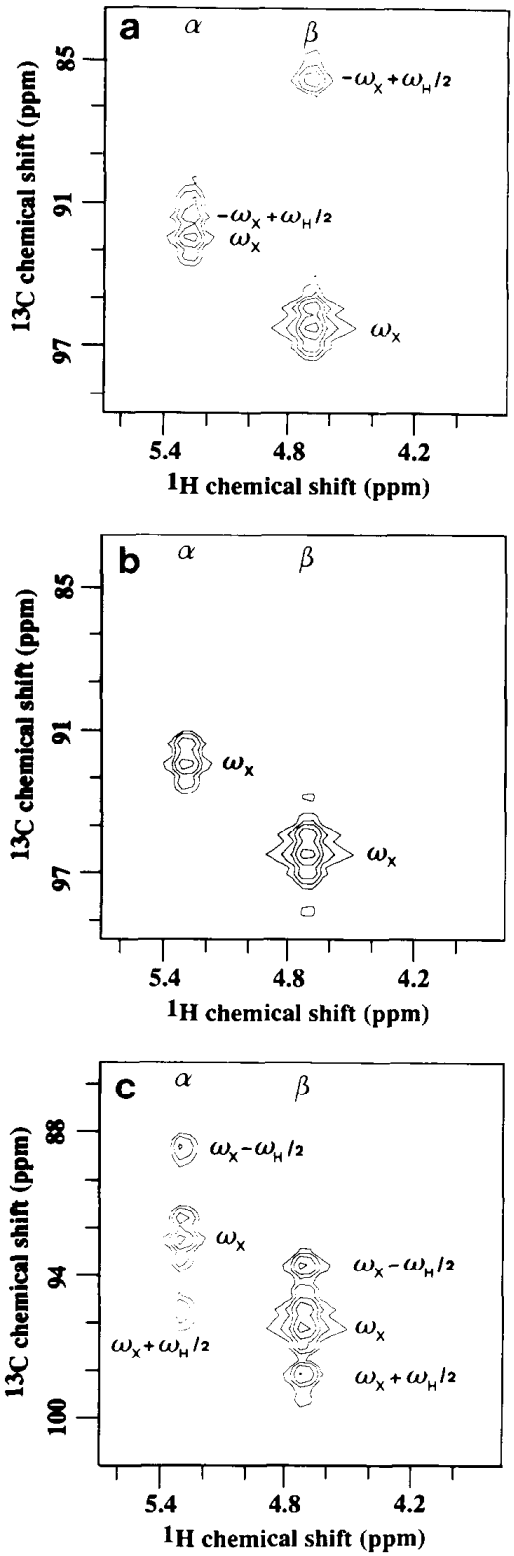

FIG. 4. Magnitude 2D ge-HSQC spectra of [$^{13}C_1$]glucose (100 mM) in 99% D_2O, showing the effect of a proton pulse with $\pi/2$ character in the middle of t_1. The gradient ratios G_1:G_2:G_3 are: (a) 2:2:−1, (b) 0:4:−1, and (c) 4:0:−1. The ^{13}C offset is 90 ppm; the ^{1}H offset 3.5 ppm.

are split into a doublet with peak separation in the order of magnitude of the heteronuclear coupling. Thus the decoupling effect of the central pulse is not effective anymore, as expected.

Phase-Sensitive Experiments

Equations [5] and [6] (HMQC) and [12] and [13] (HSQC) show that the dephasing–rephasing conditions for positive and negative heteronuclear chemical-shift evolution during t_1 are different. Since amplitude modulation in t_1 can be achieved only if both pathways are retained, it is therefore not trivial for most gradient-enhanced experiments. Although attaining amplitude modulation is not a necessary requirement for phase-sensitive detection, phasing problems (first order) due to the presence of a minimum t_1 as well as the presence of dispersion components (when a straightforward FT is used in the indirect dimensions) make it convenient to use this approach. In principle, amplitude modulation is attained when the dephasing–rephasing conditions for the two pathways have simultaneous solutions. However, solutions that satisfy Eqs. [6a] and [6b] simultaneously ($G_1 = G_2 = G_3 = 0$ and $G_1 = -G_2 = G_3/2$) also rephase signals of spins not coupled to the heteronucleus (e.g., water) and are thus not very useful. The same is true for Eqs. [13a] and [13b], which have a simultaneous solution only for $G_1 = G_2 = G_3 = 0$.

Possible approaches to attain both coherence pathways in a single scan are alternate rephasing of both pathways with gradient modulation during acquisition [SWAT; Ref. (*25*)] or avoiding dephasing during the t_1 period, e.g., in DQ-filtered COSY (*26*) or in NOESY–HMQC (*13b*). Another approach is cycling one of the gradients in two subsequent scans and adding the scans in order to detect both pathways. The effect of this method is illustrated in Figs. 5b and 5c, where spectra are shown for pathways with double-quantum dephasing (G_1:G_2:G_3 = 0:4:−5) and zero-quantum dephasing (G_1:G_2:G_3 = 0:4:−3), respectively. These dephasing–rephasing schemes by themselves

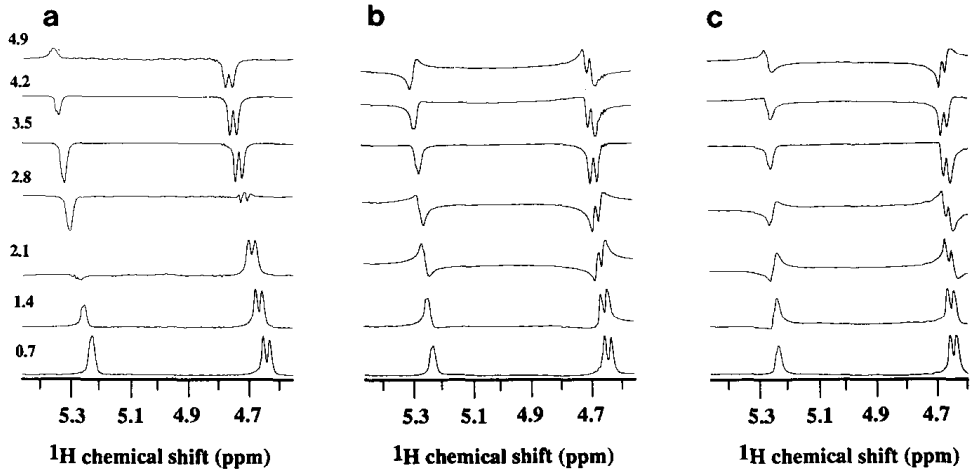

FIG. 5. Spectral modulation as a function of t_1 for (a) a two-scan gradient cycle using $G_3 = -3$ and -5, (b) $G_3 = -3$, and (c) $G_3 = -5$. $G_1 = 0$ and $G_2 = 4$ were kept constant. Note the amplitude modulation in (a) and the phase modulation in (b) and (c).

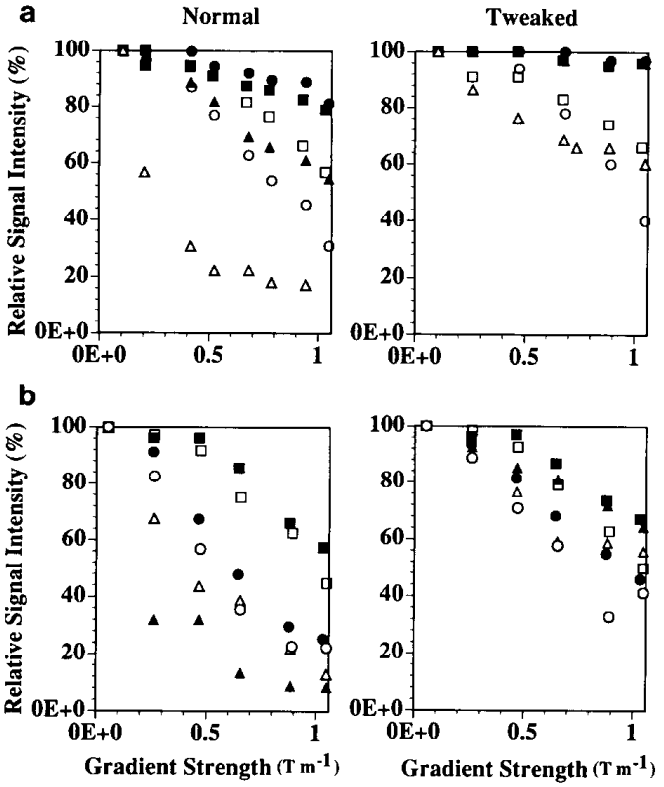

FIG. 6. HMQC signal intensity as a function of gradient strength in the x (square), y (circle), and z (triangle) directions, without (left) and with gradient tweaking (right). The gradient combinations G_1:G_2:G_3 used are: (a) 0:4:−3 (closed symbols) and 4:0:3 (open symbols) and (b) 2:2:−1 (closed symbols) and 2:2:1 (open symbols).

produce phase modulation as a function of t_1 (Figs. 5b and 5c), while their combination provides amplitude modulation (Fig. 5a). Although this approach loses the advantage of speed of single-scan techniques and a factor of two in signal-to-noise, it may be useful for studies with enough available signal-to-noise, where the advantage of frequency-independent water suppression is still needed.

Gradient Requirements

The requirements for dephasing efficiency as a function of gradient strength and the influence of B_0 inhomogeneity on this have been discussed recently (*27*). The gradient strength for our sample can be kept low, because it is in D_2O and not much dephasing power is required for suppression of unwanted coherences. In H_2O the demands are much higher and our sample provides a very suitable test case for the study of the influence of higher gradient strengths on the signal intensity.

Optimization of gradient ratios. Figures 6a and 6b show the effect of increasing gradient strength on the HMQC signal intensity for our particular experimental setup. It is clear that care must be taken when using gradients, because severe signal losses can be introduced. Several effects are clear from the figure. First, when higher gradient

strengths are used, it becomes necessary to optimize the signal rephasing by carefully adjusting (tweaking) the gradient ratios. Since the exact ratio of γ_H and γ_C is not 4, but 3.976, the correct gradient numbers should be 2.994, 5.006, and 1.006 for ZQ, DQ, and SQ (^{1}H) dephasing/rephasing, respectively. In Fig. 6 left, the uncorrected gradient ratios are used, while G_3 was adjusted for optimum rephasing in Fig. 6, right. For the ZQ dephasing/SQ ^{1}H rephasing (Fig. 6a, closed symbols), we indeed find an optimum gradient ratio G_1:G_2:G_3 = 0:4:−2.994 and the signal is completely rephased (within a few percent) for gradient strengths as high as 1 T/m. However, the optimum G_3 for the pathway of opposite sign (Fig. 6a, open symbols) was 3.005 for the x, y gradients and 2.980 for the z direction, while signal losses of 30–60% occurred for these respective directions at the highest gradient strength. We attribute this effect to eddy currents/residual gradients that persist during acquisition. The successful compensation for the 0:4:−3 combination is due to the fact that the opposite sign and small difference in magnitude of G_3 with respect to G_2 can compensate for most of the effects during acquisition. In the 4:0:3 combination, this is not possible. However, in the latter case, additional signal losses can occur due to diffusion or to inaccuracies in the proton π pulse. One combination where the influence of the latter two parameters is equal for both pathways is G_1:G_2:G_3 = 2:2:±1. Figure 6b shows that both the positive (open symbols) and negative (closed symbols) G_3 values are unable to compensate for residual gradients, with the optimum tweak values of −1.015 and 0.991 being unequal to that expected based on the gyromagnetic ratios. The situation is better for negative G_3, but in both cases the magnitude difference of G_3 with G_1 and G_2 is too large for correct compensation.

The small residual gradients experienced for the large gradient strengths in our experiments could originate from the RF coil as well as the magnet coil. Residual gradients caused by different gradient directions are expected to be different for x, y versus z due to the cylindrical symmetry of the RF coil and the magnet, which is found experimentally. When additional hardware compensation schemes (*28*) are implemented, gradient tweaking will probably not be necessary any longer. The RF coil can be improved by splitting the RF shield and by reducing the amount of conducting materials. A new coil with these features is already being designed.

Diffusion effects. The presence of pairs of pulsed gradients during periods in which transverse magnetization evolves introduces diffusion weighting and may lead to signal losses. In general, the signal attenuation for free diffusion can be described by (*29, 30*)

$$S/S_0 = e^{-\gamma^2 G^2 \tau^2 (\Delta - \tau/3) D} \qquad \text{for } \Delta \gg \tau \qquad [20a]$$

$$S/S_0 = e^{-\gamma^2 G^2 \tau^3 D} \qquad \text{for } \Delta \to \tau. \qquad [20b]$$

S and S_0 are signal intensities with and without gradients, respectively, γ is the gyromagnetic ratio (26.7519×10^7 rad T^{-1} s^{-1}), and D is the nuclear diffusion constant, which can generally be assumed equal to the molecular one. In our experiments, γ and G differ for the gradient pulses in a pair of gradients, but their product remains the same. For instance, for the gradient combination 4:0:−5, one has $(\gamma_H + \gamma_C)G_2$ and $\gamma_H G_3$, which are equal.

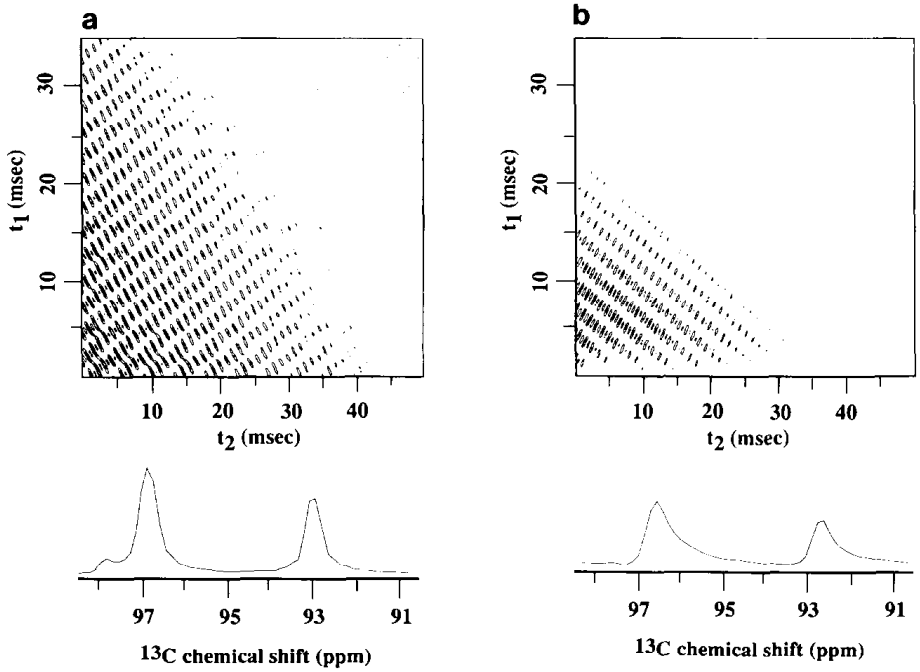

FIG. 7. (a) Two-dimensional ge-HMQC time-domain spectrum of [$^{13}C_1$]glucose for gradient selection 0:4:−5 (a) and 4:0:5 (b). The absolute-value projections of α- and β-glucose peaks on f_1 for both gradient selections are given at the bottom. The effect of t_1-dependent diffusion weighting is clearly reflected in the signal intensities. The 4:0:5 combination also shows tail-shaped resonances due to slight residual gradients. Gradient strengths used were $G_x = 0.516$ T/m, $G_y = 0.419$ T/m, and $G_z = 0.104$ T/m, for a total gradient strength of 0.673 T/m.

Depending on the gradient combination chosen, diffusion influences can drastically change the spectrum. This effect is shown in Fig. 7, where the intensity of the 2D time-domain signal is plotted as a function of t_1 for gradient combinations 0:4:−5 and 4:0:5. Two effects play a role. First, due to the presence of a minimum t_1, the signal intensities at the first value of t_1 in the 4:0:5 combination are less than those in 0:4:−5. Second, in multidimensional experiments, Δ varies as a function of t_1 for the 4:0:5 combination and a t_1-dependent diffusion weighting is introduced. Since signal intensity decreases exponentially as a function of t_1, this t_1-dependent diffusion weighting can be seen as an additional apodization of the original intensity with line broadening LB:

$$e^{-\pi \mathrm{LB} t_1} = e^{-\gamma^2 G^2 D t_1}. \qquad [21]$$

For the glucose molecule in our solution at probe temperature we determined $D = 1.17 \times 10^{-9}$ m^2 s^{-1} using a simple diffusion-weighted spin-echo experiment. This D value should lead to an initial signal loss of 9% for combination 4:0:5 (Eq. [20a]) with respect to 0:4:−5 (Eq. [20b]) for the gradient values in the legend to Fig. 7. It should be kept in mind that we use sinusoidal gradients and that the actual gradient strength must be multiplied by a factor $2/\pi$ to obtain the correct G for Eq. [20]. The expected line broadening can be calculated to be 14 Hz, in good correspondence with

experiment, where a broadening of about 13 Hz is found. The total signal intensity drop due to line broadening (original linewidth, 52 Hz; final, 65 Hz) and the initial loss should be about 29%. We find about 41% in the data. We attribute this extra drop to some residual gradient effects, whose presence is reflected in the asymmetrical lineshapes. The intensity drop in the time-domain plots agrees qualitatively with the calculated ones: at point 128 of 256 points we calculate an intensity of 53% of the value of the first point (a dwell time of 140 μs was used). Combined with the 9% initial drop, the agreement with experiment is good.

The diffusion effects will be most pronounced for small molecules. For instance, water-suppression becomes more efficient at longer t_1, which may cause t_1-dependent baseline modulation. However, since suppression due to gradient coherence selection is usually very effective, this baseline effect is probably not very important. The diffusion weighting will generally not be large enough to cause significant signal loss for macromolecules.

The additional gradients G_{a1} in the HMQC sequence can introduce severe t_1-dependent diffusion weighting and should be avoided when studying small molecules or adjusted as a function of t_1 to compensate for increasing diffusion time. The gradient pairs G_{a1} and G_{a2} in the HSQC experiment have only a very short time between dephasing and rephasing and do not vary as a function of t_1. Their contribution to diffusion weighting is therefore generally negligible.

Locking and spinning. An additional effect of strong pulsed gradients on the NMR experiment is a dephasing of the lock signal during the pulses. However, we found experimentally that the lock is able to recover during the periods between scans and is not lost. Gradient effects may also cause incoherent frequency shifts of the lock signal, but no significant t_1 noise was found in our experiments. Thus, it does not seem to be necessary to gate the lock, although this would be a better approach. Two of the factors that are important in enabling locking without gating are the high quality of the gradients (small residual gradients with short time constants) and the fact that dephasing for deuterium is a factor of 6.5 smaller than that for protons, due to the difference in gyromagnetic ratio.

All reported experiments were performed nonspinning. In principle, when only z gradients are used, it should be possible to spin as long as there is no motion in the z direction. With our present probe setup we cannot yet test this hypothesis.

Multiple gradient directions. The question often arises if it is sufficient to have only one gradient direction when performing gradient-enhanced spectroscopy. For instance, only a z gradient could suffice for spoiling, since this is the most effective direction due to the dimensions of the NMR tube. However, it may be important to have multiple gradient directions if interscan gradient-recalled echoes (e.g., those occurring in experiments with short repetition times) are rephasing the previously coherently spoiled resonances. Interscan echoes can be avoided by cycling gradient directions from scan to scan, which of course does not add to the experiment time (*13b*). It is also convenient to have more gradient directions when multiple gradient functions are necessary, e.g., for coherence selection, spoiling and diffusion. In diffusion experiments, which can be useful for studying proton exchange (*31*) and motion of macromolecules, x, y, and z gradients are equally effective, since dephasing depends on microscopic displacements. To avoid interference between spoiling and diffusion gra-

dients in gradient-enhanced NOESY (*31*) or stimulated echo (*5*) experiments, it will therefore be best to use the z gradient for signal dispersion during the mixing time and x or y gradients for diffusion weighting.

CONCLUSIONS

We have presented an overview of gradient methods for heteronuclear correlation spectroscopy (ge-HMQC and ge-HSQC) and compared them with conventional experiments. Gradient-enhanced experiments detect only a single coherence pathway and have the disadvantage of losing a factor of 2 in signal per scan. However, since phase-sensitive experiments using the States method or TPPI also select only for one pathway, equal amounts of signals are detected in a multiscan experiment. On the other hand, absolute-value processing is mandatory in many gradient-enhanced experiments, resulting in resolution loss. The most important feature of gradient-enhanced experiments is coherence selection with efficient frequency-independent water suppression in a single scan. This may for instance be useful for kinetic experiments, where time resolution is essential. Phase-cycle experiments have the disadvantage that the process of subtraction may not be as perfect as desirable, causing t_1 noise and the presence of baseline artifacts. The occurrence of artifacts due to imperfections of the π pulse in the middle of t_1 was checked for the conventional and gradient-enhanced methods, and it was found that the gradients do not introduce additional resonances. The fact that spectra without artifacts can be selected using specific gradient combinations may be important in the interpretation of dubious cross peaks.

We have shown the possibility of attaining phase-sensitive spectra in two-scan experiments adding different dephasing–rephasing pathways.

Increasing gradient strengths may cause a dramatic signal loss when the gradients are not adjusted exactly, e.g., for the correct ratio of gyromagnetic ratios. With correct tweaking, our high-quality gradients gave excellent results for gradient strengths as high as 1 T/m. For some gradient combinations, residual gradients persisting through acquisition could not be completely compensated and showed reduced signal intensity. Incremental diffusion weighting as a function of t_1 may also produce severe signal loss.

The choice of a certain combination depends on the experiment that must be performed. For convenience of the reader, Table 5 summarizes the most important aspects for both ge-HMQC and ge-HSQC. One column is added for the percentage of the maximum gradient strength available to dephase unwanted coherences that experience a normal spin-echo sequence, e.g., water. For instance, for G_1:G_2:G_3 = 3:5:0 in the HMQC sequence, the available power strength per unit is 40%. The refocusing central π pulse changes the sign of the evolving coherence and a 3:3:0 combination would refocus all water. So, two units on a maximum of 5 (40%) are available for dephasing of unwanted coherences. Since residual gradients are negligible for high-quality gradients, the best combinations for HMQC are G_1:G_2:G_3 = 3:5:0 and 5:3:0. In these combinations no diffusion weighting is induced when G_1 and G_2 are placed directly around the proton 7 pulse, and no artifacts are visible. One potential disadvantage of these two combinations is that the phase-sensitive SWAT method cannot be used, but the other phase-sensitive approaches are still applicable. For HSQC spectroscopy, G_1:G_2:G_3 = 0:4:±1 are most suitable. The HSQC sequences have higher dephasing

TABLE 5

Summary of Characteristics for ge-HMQC and ge-HSQC

Gradient combinations $G_1:G_2:G_3$	Sensitivity to residual gradients	Diffusion weighting (t_1-dependent)	Artifacts (due to π pulse inaccuracy)		% maximum gradient strength (for dephasing water)
			Cross peaks	Multiplets[a]	
		HMQC			
2:2:1	++	Yes	No	No	50
2:2:−1	+	Yes	Yes	No	50
0:4:−3	−	No	Yes	No	25
0:4:−5	−	No	Yes	No	20
4:0:3	++	Yes	No	No	25
4:0:5	++	Yes	No	No	20
3:5:0	++	No	No	No	40
5:3:0	++	No	No	No	40
		HSQC			
0:4:1	++	No	No	Yes	100
0:4:−1	+	No	No	Yes	60
4:0:1	++	Yes	Yes	Yes	60
4:0:−1	+	Yes	Yes	Yes	100
2:2:1	++	Yes	Yes	Yes	50
2:2:−1	+	Yes	Yes	Yes	50

[a] Multiplets at the normal frequency due to the fact that the *J*-coupling evolution is not refocused.

Note. Gradient combinations and dephasing efficiencies are for ^{13}C ($\gamma_H:\gamma_X = 4:1$); for ^{15}n ($\gamma_H:\gamma_X = 9.88:1$) dephasing efficiencies are much lower, except for the 100% cases.

efficiency, but are more susceptible to signal losses than the HMQC methods, mainly due to the larger number of RF pulses used.

In summary, gradient-enhanced heteronuclear NMR provides an excellent alternative to phase cycling and may be advantageous for several experiments, especially when time resolution is essential and when efficient frequency-independent water suppression is required. It will certainly take an important place in 2D, 3D, and 4D studies of large macromolecules.

APPENDIX

The coherence-transfer formalism (*19, 20*) uses shift operators, otherwise known as raising and lowering operators. These operators are related to the angular momentum operators by

$$I^+ = I_x + iI_y \qquad [22a]$$

$$I^- = I_x - iI_y. \qquad [22b]$$

Using this formalism, it is easier to see how a particular coherence-transfer pathway can be selected by gradients (Eq. [1]). The effects of chemical shift, spin coupling, and radiofrequency pulses with flip angle β on the magnetization are

$$\text{chemical shift:} \quad I^p \xrightarrow{\omega_I t I_z} I^p e^{-ip\omega_I t} \qquad [23]$$

$$\text{spin coupling:} \quad I^+ \xrightarrow{\pi Jt 2 I_z S_z} I^+ \cos(\pi Jt) - 2iI^+ S_0 \sin(\pi Jt) \qquad [24a]$$

$$I^- \xrightarrow{\pi Jt 2 I_z S_z} I^- \cos(\pi Jt) + 2iI^- S_0 \sin(\pi Jt) \qquad [24b]$$

$$\text{radio frequency:} \quad I^+ \xrightarrow{\beta I_x} 1/2[I^+(\cos\beta + 1)] + I_0(i \sin\beta) - 1/2[I^-(\cos\beta - 1)] \qquad [25a]$$

$$I^- \xrightarrow{\beta I_x} 1/2[I^-(\cos\beta + 1)] - I_0(i \sin\beta) - 1/2[I^+(\cos\beta - 1)] \qquad [25b]$$

$$I_0 \xrightarrow{\beta I_x} i/2(I^+ \sin\beta) + I_0 \cos\beta - i/2(I^- \sin\beta) \qquad [25c]$$

$$I_0 \xrightarrow{\beta I_y} 1/2(I^+ \sin\beta) + I_0 \cos\beta + 1/2(I^- \sin\beta). \qquad [25d]$$

ACKNOWLEDGMENTS

This research was financially supported by PharmaGenics, Inc., and the Netherlands Foundation for Chemical Research (SON) with aid of the Netherlands Organization of Scientific Research (NWO). The shielded gradients that made this study possible were provided by GE NMR Fremont. We thank Dr. Ralph Hurd (GE Fremont) for valuable discussions and suggestions. J.R.C. thanks the Spanish Ministerio de Educación y Ciencia and Fulbright Commission for funding with a postdoctoral fellowship. G.W.V. acknowledges financial support from the Netherlands Organization for Scientific Research (NWO). The $^{13}C_1$ glucose was provided by Cambridge Isotopes. We thank María José Subiela for preparing the figures.

REFERENCES

1. (*a*) A. A. MAUDSLEY, A. WOKAUN, AND R. R. ERNST, *Chem. Phys. Lett.* **55,** 9 (1978); (*b*) A. BAX, P. G. DE JONG, A. F. MEHLKOPF, AND J. SMIDT, *Chem. Phys. Lett.* **69,** 567 (1980); (*c*) C. J. R. COUNSELL, M. H. LEVITT, AND R. R. ERNST, *J. Magn. Reson.* **64,** 470 (1985); (*d*) P. BARKER AND R. FREEMAN, *J. Magn. Reson.* **64,** 334 (1985).
2. C. H. SOTAK AND D. FREEMAN, *J. Magn. Reson.* **77,** 382 (1988); C. H. SOTAK, D. FREEMAN, AND R. E. HURD, *J. Magn. Reson.* **78,** 355 (1988).
3. (*a*) A. KNÜTTEL AND R. KIMMICH, *J. Magn. Reson.* **83,** 335 (1989); (*b*) *Magn. Reson. Med.* **9,** 254 (1989); (*c*) *J. Magn. Reson.* **81,** 570 (1989); (*d*) *Magn. Reson. Med.* **10,** 404 (1989).
4. D. M. DODDRELL, I. M. BRERETON, L. N. MOXON, AND G. J. GALLOWAY, *Magn. Reson. Med.* **9,** 132 (1989).
5. (*a*) P. C. M. VAN ZIJL, C. T. W. MOONEN, J. R. ALGER, J. S. COHEN, AND A. S. CHESNICK, *Magn. Reson. Med.* **10,** 256 (1989); (*b*) C. T. W. MOONEN, P. C. M. VAN ZIJL, J. GILLEN, P. DALY, M.

VON KIENLIN, J. S. COHEN, AND G. WOLF, *NMR Biomed.* **2,** 201 (1989); (*c*) C. T. W. MOONEN AND P. C. M. VAN ZIJL, *J. Magn. Reson.* **88,** 28 (1990).
6. L. A. TRIMBLE, J. F. SHEN, A. H. WILMAN, AND P. S. ALLEN, *J. Magn. Reson.* **86,** 191 (1990).
7. R. E. HURD, *J. Magn. Reson.* **87,** 422 (1990).
8. M. VON KIENLIN, C. T. W. MOONEN, A. VAN DER TOORN, AND P. C. M. VAN ZIJL, *J. Magn. Reson.* **93,** 423 (1991).
9. I. M. BRERETON, S. CROZIER, J. FIELD, AND D. M. DODDRELL, *J. Magn. Reson.* **93,** 54 (1991).
10. (*a*) A. KNÜTTEL, R. KIMMICH, AND K.-H. SPOHN, *J. Magn. Reson.* **86,** 526 (1990); (*b*) A. KNÜTTEL, K.-H. SPOHN, AND R. KIMMICH, *Magn. Reson. Med.* **17,** 470 (1991).
11. S. SWANSON AND H. N. YEUNG, *in* "Proceedings, 31st Experimental NMR Conference," p. 197, 1990.
12. (*a*) R. E. HURD AND B. K. JOHN, *J. Magn. Reson.* **91,** 648 (1991); (*b*) *J. Magn. Reson.* **92,** 658 (1991); (*c*) B. K. JOHN, D. PLANT, S. L. HEALD, AND R. E. HURD, *J. Magn. Reson.* **94,** 664 (1991).
13. G. W. VUISTER, R. BOELENS, R. KAPTEIN, R. E. HURD, B. JOHN, AND P. C. M. VAN ZIJL, *J. Am. Chem. Soc.*, **113,** 9688 (1991).
14. P. C. M. VAN ZIJL AND C. T. W. MOONEN, *in* "NMR, Basic Principles and Progress" (J. Seelig and M. Rudin, Eds.), Vol. 26, pp. 67–108, Springer-Verlag, Berlin/Heidelberg, 1992.
15. (*a*) L. J. MÜLLER, *J. Am. Chem. Soc.* **101,** 4481 (1979); (*b*) A. BAX, R. H. GRIFFEY, AND B. L. HAWKINS, *J. Am. Chem. Soc.* **105,** 7188 (1983); (*c*) A. BAX, R. H. GRIFFEY, AND B. L. HAWKINS, *J. Magn. Reson.* **55,** 301 (1983); (*d*) M. R. BENDALL, D. T. PEGG, AND D. M. DODDRELL, *J. Magn. Reson.* **52,** 81 (1983).
16. G. BODENHAUSEN AND D. J. RUBEN, *Chem. Phys. Lett.* **69,** 185 (1980).
17. E. R. P. ZUIDERWEG, *J. Magn. Reson.* **86,** 346 (1990).
18. A. BAX, M. IKURA, L. E. KAY, D. A. TORCHIA, AND R. TSCHUDIN, *J. Magn. Reson.* **86,** 304 (1990).
19. (*a*) G. BODENHAUSEN, H. KOGLER, AND R. R. ERNST, *J. Magn. Reson.* **58,** 370 (1984); (*b*) N. MÜLLER, G. BODENHAUSEN, AND R. R. ERNST, *J. Magn. Reson.* **75,** 297 (1987).
20. A. D. BAIN, *J. Magn. Reson.* **56,** 418 (1984).
21. G. J. BARKER AND T. H. MARECI, *J. Magn. Reson.* **83,** 11 (1989).
22. G. A. MORRIS AND R. FREEMAN, *J. Am. Chem. Soc.* **101,** 760 (1979).
23. (*a*) A. BAX, M. IKURA, L. E. KAY, D. A. TORCHIA, AND R. TSCHUDIN, *J. Magn. Reson.* **86,** 304 (1990); (*b*) A. G. PALMER III, J. CAVANAGH, P. E. WRIGHT, AND M. RANCE, *J. Magn. Reson.* **93,** 151 (1991).
24. D. MARION, M. IKURA, R. TSCHUDIN, AND A. BAX, *J. Magn. Reson.* **85,** 393 (1989).
25. R. E. HURD, B. K. JOHN, AND H. D. PLANT, *J. Magn. Reson.* **93,** 666 (1991).
26. A. L. DAVIS, E. D. LAUE, J. KEELER, D. MOSKAU, AND J. LOHMAN, *J. Magn. Reson.* **94,** 637 (1991).
27. C. T. W. MOONEN, G. SOBERING, P. C. M. VAN ZIJL, J. GILLEN, AND A. BIZZI, *J. Magn. Reson.* **98,** 556 (1992).
28. M. VON KIENLIN, K. HEDGES, AND A. OLSON, *in* "Proceedings, 31st Experimental NMR Conference," p. 166, 1990.
29. E. O. STEJSKAL AND J. E. TANNER, *J. Chem. Phys.* **42,** 288 (1965).
30. P. C. M. VAN ZIJL AND C. T. W. MOONEN, *J. Magn. Reson.* **87,** 18 (1990).
31. C. T. W. MOONEN, P. VAN GELDEREN, G. VUISTER, AND P. C. M. VAN ZIJL, *J. Magn. Reson.* **97,** 419 (1992).